PRAMANA — journal of physics
© Indian Academy of Sciences
Vol. 53, No. 6
December 1999
pp. 1–11

Global variables and identified hadrons in the PHENIX experiment

John P. Sullivan for the PHENIX collaboration
P-25 MS-H846, Los Alamos National Lab, Los Alamos, NM 87545, USA

Abstract. PHENIX measurements related to global variables and identified hadrons are discussed. These include two-pion correlations, elliptic flow, and $dN/d\eta$. Measurements of event-by-event fluctuations in mean transverse momentum, mean transverse energy, and net charge are presented for particles within the PHENIX acceptance. The centrality dependence of these measurements is also discussed.

Keywords. RHIC, global variables, fluctuations, two-pion correlations

PACS Nos 2.0

1. Introduction

This paper summarizes some of the results from the first year of running the PHENIX experiment at RHIC. The center of mass energy per nucleon for all the data in this paper was $\sqrt{s_{NN}}$ = 130 GeV. Two-pion correlations ($\pi^+\pi^+$ and $\pi^-\pi^-$), elliptic flow, and $dN/d\eta$ measurements are discussed. Measurements event-by-event fluctuations in mean transverse momentum, mean transverse energy, and net charge are presented for particles within the PHENIX acceptance. In most cases, the centrality dependence of the measurements is discussed.

Other talks at this conference summarized the PHENIX results for high p_T charged hadrons and π^0's [1], the transverse momentum spectra for identified hadrons [2], and $dN/d\eta$ measurements versus centrality [3].

2. The PHENIX detector

The PHENIX detector at RHIC was designed to measure a variety of hadron, photon, and lepton observables. The major goal of the heavy ion program in PHENIX is to detect and characterize the quark gluon plasma. The design philosophy is based on the assumption that detecting and characterizing the quark gluon plasma will require the widest possible variety of measurements.

Details of the PHENIX detector design and construction can be found in published PHENIX papers [4–6]. Here, a brief description of some of the relevant parts of the detector is given.

The trigger and centrality selection are based on the Beam-Beam Counters (BBC) and the Zero Degree Calorimeter (ZDC). The BBC consists of two arrays of 64 quartz Cherenkov radiators connected to photomultiplier tubes. They cover 2π in azimuth and $3.0< \eta <3.9$. The primary interaction trigger required at least two PMT's to fire in each BBC array. Based on detailed simulations, this trigger reflects $92\pm2\%$ of the nuclear interaction cross section. The ZDC is a pair of small calorimeters ±18.25 m from the interaction region. They measure neutrons within 2 mr of the beam direction ($|\eta| >6$). The ZDC was used to generate a second interaction trigger, which is sensitive to the combined nuclear interaction and mutual Coulomb dissociation cross sections. For details see [4].

The centrality selection is based on a two-dimensional plot of the signal in the ZDC vs. the summed analog signal from all of the BBC PMT's. The top half of figure 1 shows the centrality cuts on this two-dimensional plot. The bottom half of the plot shows the minimum bias distribution of the number of tracks in the central arms, using an analysis based on PC1 and PC3 [3,4]. The multiplicity distributions for the four most central multiplicity bins (shown on the upper half of the plot) are also given.

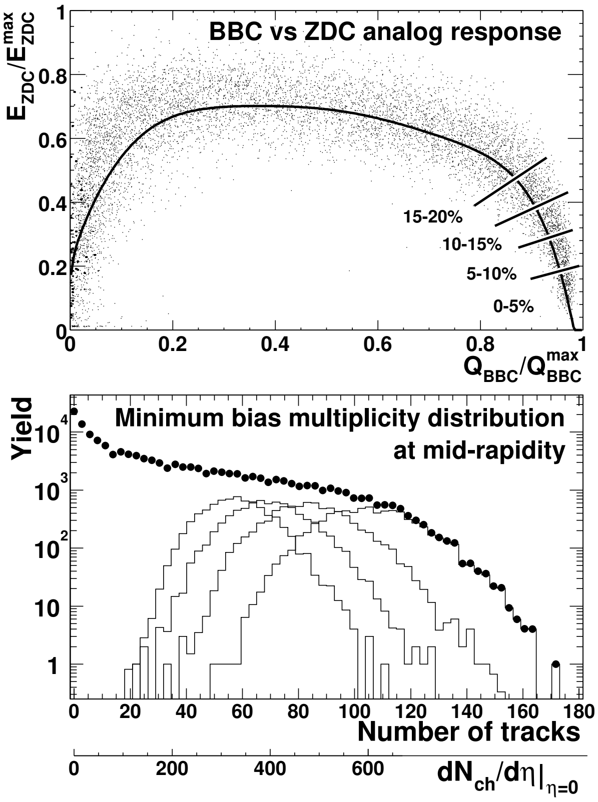

Figure 1. The top half shows the two-dimensional plot of ZDC signals vs. BBC signal and some of the more central centrality cuts. The bottom half of the plot shows the minimum bias multiplicity distribution and the multiplicity distribution for some of the centrality cuts.

The central arms of PHENIX were not completely instrumented in the first year of RHIC

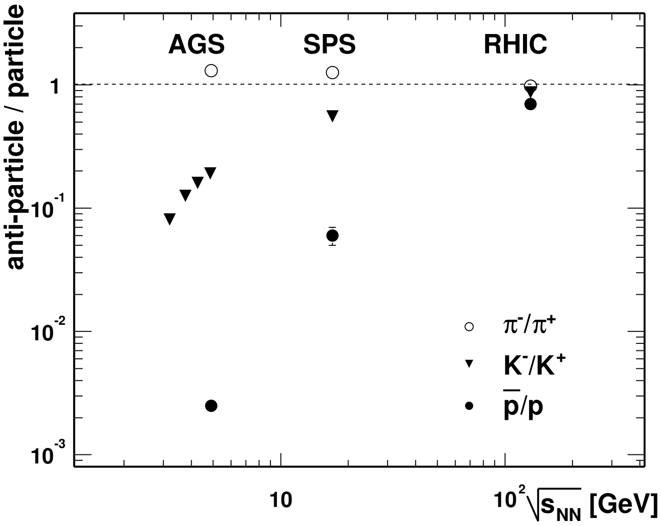

Figure 2. Anti-particle/particle ratios vs. $\sqrt{s_{NN}}$. The "RHIC" data are PHENIX preliminary.

running. Moving outward radially, a fully instrumented arm would have a Drift Chamber (DC), followed by Pad Chamber 1 (PC1), a Ring Imaging Cherenkov (RICH), a Time Expansion Chamber (TEC), Pad Chamber 3 (PC3), a Time-of-Flight (TOF) wall, followed by either a Lead Glass (PbGl) or a Lead Scintillator (PbSc) calorimeter. The TOF system covers only part of one arm's acceptance. The RICH, PbGl, and TEC were not used in the analyses described here. Measured radially from the beam line, the drift chambers were at $2.0\,\mathrm{m} < r < 2.4\,\mathrm{m}$. PC1 and PC3 were at 2.49 m and 4.98 m, respectively. The TOF wall was at r = 5.06 m and and front face of the PbSc was 5.1 m from the beam axis. The PbSc calorimeter has an energy resolution of $8.2\%/\sqrt{E(\mathrm{GeV})}\oplus 1.9\%$. $0.3 \leq E_e \leq 40.0$ GeV [7].

3. Results

3.1 Anti-particle/particle ratios

The transverse momentum spectra (and the ratios of these spectra) of identified hadrons are based on tracking in the central arms of PHENIX using the DC and PC1. The momentum resolution is $\delta p/p = 0.6\% \oplus 3.6\% p$. A measurement of the time-of-flight using the BBC as a start time and the TOF as a stop time is used to determine the particle velocity. The time resolution for this system was ≈ 115 ps.

As noted in another PHENIX talk at this conference [2], the net number of baryons (baryons - anti-baryons) at midrapidity is smaller than at lower energies. This is partially due to the increased number of anti-baryons at $\sqrt{s_{NN}}$ = 130 GeV. In fact, this is an interesting and general feature of particle/anti-particle ratios at RHIC when compared to either SPS or AGS data. All of these particle/anti-particle ratios are closer to 1 than at lower

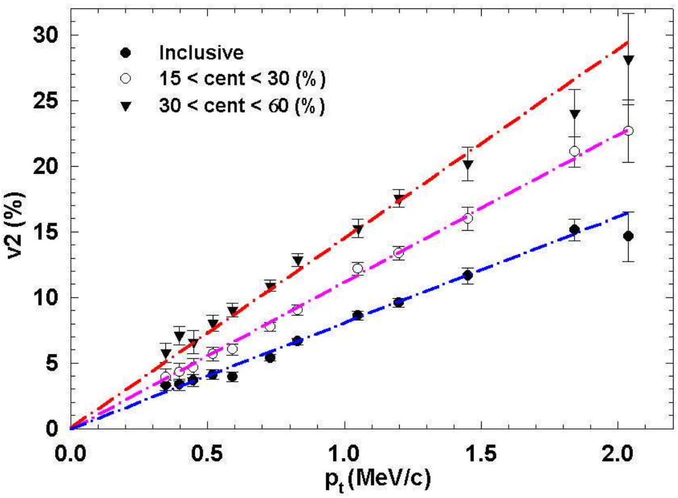

Figure 3. v_2 vs. p_T for three centrality bins.

energies. The π^-/π^+ ratio is slightly less and the K^-/K^+ and $\overline{p}/p$ ratios have risen significantly. All are closer to one. This is shown in figure 2, which compares PHENIX preliminary data to SPS and AGS results. Qualitatively, this is easy to understand. At $\sqrt{s_{NN}}$ = 130 GeV the number of produced particles is much larger than the initial number of particles and the anti-particle/particle ratios are less sensitive to the initial system.

3.2 Elliptic flow

Elliptic flow is detected via an anisotropy in the azimuthal distribution of emitted particles. One technique used in elliptic flow analysis [8,9] is a Fourier decomposition of the azimuthal angle difference ($\Delta\phi$) between pairs of emitted particles,

$$\frac{dN}{d\Delta\phi} \propto (1 + \sum_{n=1}^{\infty} 2v_n^2 \cos(n\Delta\phi)). \tag{1}$$

With this method, which assumes that flow is the dominant cause of the azimuthal correlations, the magnitude of the elliptic flow is measured by v_2^2 in equation 1. This method allows the elliptic flow to be measured without an event-by-event determination of the reaction plane.

Figure 3 shows PHENIX preliminary data for v_2 vs. the mean transverse momentum of the detected particles for two centrality bins along with the inclusive (no centrality selection) data. v_2 is relatively large and increases approximately linearly with p_T and decreases for more central collisions. v_2 should approach zero for b=0 and for the most peripheral collisions since no reaction plane can be defined in these cases. Similarly, it should approach zero as p_T approaches zero. These preliminary data are consistent with measurements from STAR [10] and PHOBOS [11]. The results suggest that the high-energy-density matter created in the collisions at RHIC efficiently translates the initial spacial asymmetry in the collisions into a similar asymmetry in momentum space. The p_T dependence is consistent with the development of strong transverse velocity fields in the high-density matter, which is in turn consistent with the development of large pressures in the collision zone.

3.3 Two-pion correlations

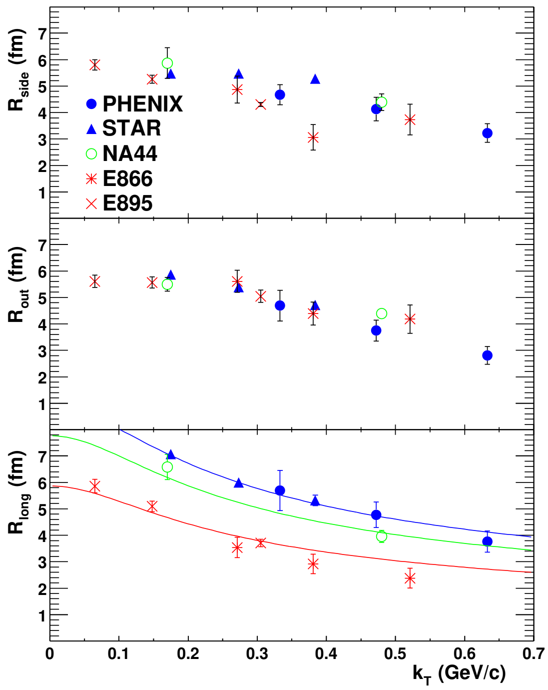

Figure 4. Correlation function radius parameters vs. $\sqrt{s}$.

Two-pion correlations have become a standard technique for probing the size of the collision zone. PHENIX has measured $\pi^+\pi^+$ and $\pi^-\pi^-$ correlation functions [12]. The correlation functions are fit to an equation of the form [13,14]:

$$C_2 = 1 + \lambda \exp(-R_L^2 q_L^2 - R_S^2 q_S^2 - R_O^2 q_O^2) \tag{2}$$

where q_L is the momentum difference along the beam direction, q_O is parallel to the mean momentum of the pair ($k_T = (p_{T1} + p_{T2})/2$), and q_S is perpendicular to q_L and q_O. The correlation function is calculated in the longitudinal co-moving system (LCMS), which is the frame in which the longitudinal pair velocity vanishes.

As with the single hadrons, the two-pion correlation analysis finds tracks and their momenta in one of the central arms of PHENIX using DC and PC1. The momentum resolution is $\delta p/p = 0.6\% \oplus 3.6\% p$. A measurement of the time-of-flight using the BBC as a start time and the PbSc calorimeter as a stop time is used to determine the particle velocity. The time resolution for this system was $\approx$ 600 ps. The TOF system (which was used for the ratios of identified single hadrons above) has better time resolution, but a smaller geometrical acceptance. The PbSc system was used in the two-particle correlation analysis because the larger acceptance of the PbSc proved more important than the better resolution of the TOF system. For further details on this analysis, see [12].

Figure 4 shows compares some measurements of radius parameters from the AGS ($\sqrt{s_{NN}}$=4.9 and 4.1 GeV) [16,17], the SPS ($\sqrt{s_{NN}}$=17.3 GeV) [15] to the PHENIX [12] and STAR data [18] at at $\sqrt{s_{NN}}$=130 GeV. The SPS data are for Pb+Pb collisions, all other other data are for Au+Au. The transverse radii R_O and R_S show no clear variation with collision energy. $R_O \approx R_S$ in all cases. This result is surprising given the factor of $\sim$3 change in the total charged particle multiplicity per unit rapidity at mid-rapidity [19]. There is a significant variation in R_L with collision energy. The curves on the bottom panel of figure 4 show fits of the R_L dependence to $A/\sqrt{m_T}$ [20,21] for the three sets of beam energies. The results of these fits allow us to quantify the beam energy dependence. The fits give: $A = 3.32 \pm 0.03$, 2.9 ± 0.1, and 2.19 ± 0.05 fm$\cdot$GeV$^{\frac{1}{2}}$ for $\sqrt{s_{NN}} = 130$, 17.3, and 4.1–4.9 GeV respectively.

PHENIX and STAR data in Figure 4, overlap in k_T, with the STAR data starting at lower k_T and the PHENIX data extending to high k_T. In the overlap region, the data points agree within uncertainties.

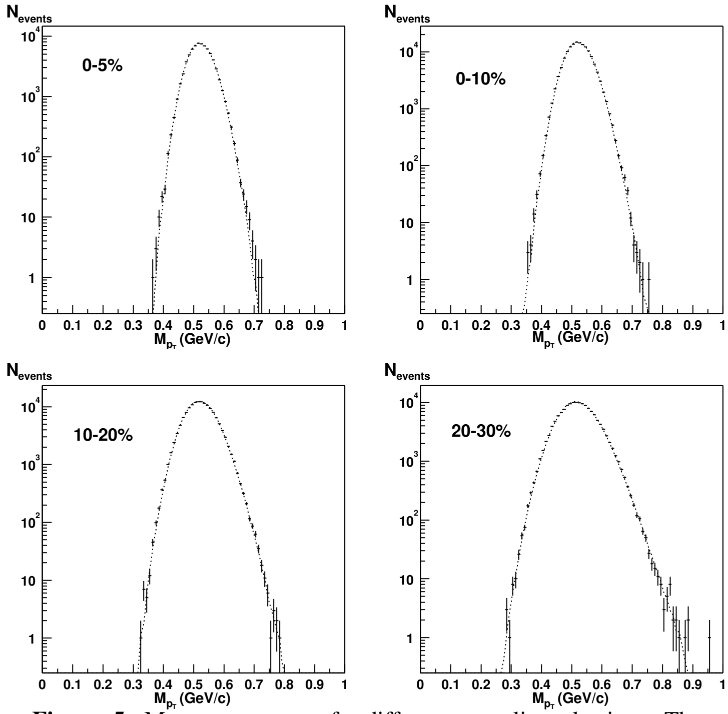

Figure 5. Mean p_t per event for different centrality selections. The curves are from mixed events. The data are PHENIX preliminary.

3.4 p_T and e_T fluctuations

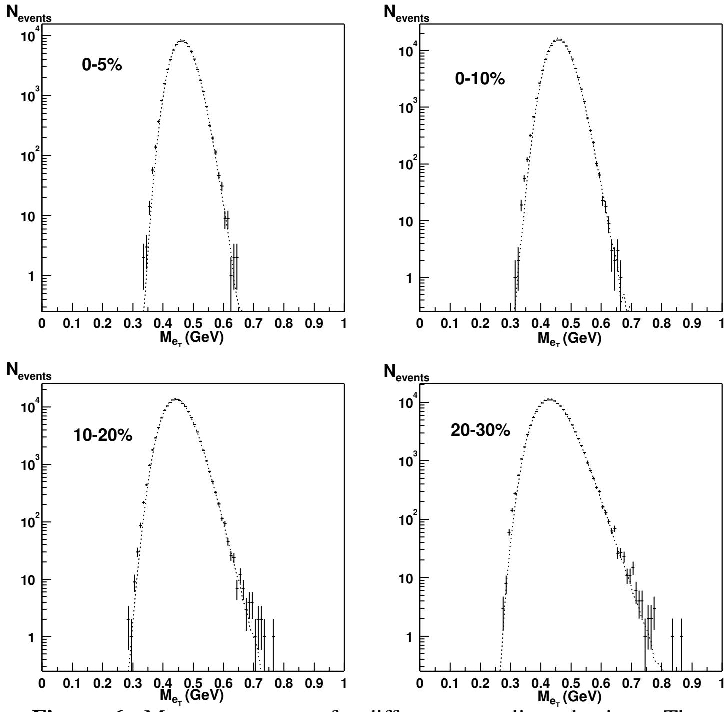

Figure 6. Mean e_t per event for different centrality selections. The curves are from mixed events. The data are PHENIX preliminary.

Instabilities of various origins [22–24] near the QCD phase transition can cause non-statistical fluctuations in observables in heavy ion collisions [25]. To find evidence for such effects, event-by-event distributions of the mean transverse momentum (M_{pT}) and mean transverse energy (M_{eT}) were measured. These distributions are then compared to distributions assuming statistically independent particle emission to search for evidence of non-statistical fluctuations.

M_{pT} is calculated for each event as

$$M_{pT} = (1/N_{tracks}) \sum_{i=1}^{N_{tracks}} p_{Ti}, \tag{3}$$

where N_{tracks} is the number of good tracks in the fiducial volume with 0.2< p_T <1.5 GeV/c. The measurement of M_{pT} used tracks reconstructed used a portion of the DC and PC1 with $\Delta\phi = 58.5°$ and $|\eta| < 0.35$. This fiducial volume was selected to minimize the effects of time dependent variations in the DC performance during the run. No acceptance or efficiency corrections are applied to M_{pT} because they do not vary from event-to-event and are the same for data and mixed events. The M_{eT} distribution is calculated using:

Table 1. Mean number of tracks and fluctuation quantities for the M_{pT} analysis. The results are PHENIX preliminary.

Centrality class	$< N_{tracks} >$	F_T (%)	ϕ_{p_T} (MeV/c)
0 - 5 %	59.6	1.9 ± 2.1	5.65 ± 6.02
0 - 10 %	53.9	2.0 ± 2.5	6.03 ± 7.28
10 - 20 %	36.6	2.1 ± 2.2	6.11 ± 6.63
20 - 30 %	25.0	1.8 ± 3.0	5.47 ± 9.16

$$M_{eT} = (1/N_{clus}) \sum_{i=1}^{N_{clus}} e_{Ti}, \tag{4}$$

where N_{clus} is the number of calorimeter clusters with $0.225 < e_T < 2.0$ GeV. Additional cuts required a minimum number of tracks (for M_{pT}) or clusters (for M_{eT}) were used to insure enough tracks/clusters to determine a mean and to eliminate background.

Mixed event distributions are used as the baseline for statistically independent particle emission. The same cuts as are used in real events are applied to mixed events. Only events with the same number of tracks/clusters were mixed. Only one e_T or p_T per real event was included. Only events from the same centrality class were mixed.

Figures 5 and 6 show the M_{pT} and M_{eT} distributions, respectively. The points with error bars are the data. The curves are from mixed events. The real and mixed events agree well for M_{pT}. For M_{eT}, the data distribution is slightly wider at the lower M_{eT} edge. Monte Carlo studies show that part of this difference is due to cluster merging in the calorimeter. Simulations suggest that the remaining difference is probably due background from low energy electrons and muons which scatter off of the central magnet pole faces into the acceptance. Because of the difficulty quantifying this contribution, the present results should be taken as an upper limit to the non-statistical fluctuations.

To quantify any fluctuations in excess of the baseline, define $\omega_T = \sigma_{M_T}/ < M_T >$, where M_T can be either M_{pT} or M_{eT} and σ_{M_T} is the rms width of the distribution. If the difference in the fluctuations from a random baseline is $d = \omega_T(data) - \omega_T(baseline)$, then the magnitude of any excess fluctuations can be defined as the fraction of the fluctuation which is not due to statistically independent particle emission:

$$F_T = \frac{\omega_T(data) - \omega_T(baseline)}{\omega_T(baseline)} = \frac{\sigma_T(data) - \sigma_T(baseline)}{\sigma_T(baseline)} \tag{5}$$

F_T is related to the quantity ϕ_T, which has been used in other analyses [26,27]:

$$\phi_T = F_T \sigma_T(baseline) \sqrt{< N_T >} \tag{6}$$

where $< N_T >$ is the mean number of tracks in the detector's acceptance. An advantage of F_T over ϕ_T is that measurements can be compared without scaling by the number of tracks in the detector's acceptance.

Tables 1 and 2 summarize some of the fluctuation quantities for M_{pT} and M_{eT}, respectively. For p_T, the values of F_T are all $\approx 1\sigma$ above zero in each case. Perhaps this is an effect of two-particle correlations. The e_T results are farther from zero, but part of this effect is caused by cluster merging, part is probably caused by background, and part should be caused by two-particle correlations. The results should be taken as upper limits.

Table 2. Mean number of tracks and fluctuation quantities for the M_{eT} analysis. The results are PHENIX preliminary.

Centrality class	$< N_{clus} >$	F_T (%)	ϕ_{eT} (MeV)
0 - 5 %	68.6	4.3 ± 1.3	11.5 ± 3.59
0 - 10 %	62.1	5.0 ± 1.6	13.6 ± 4.23
10 - 20 %	41.6	4.2 ± 2.2	11.1 ± 5.75
20 - 30 %	28.0	3.5 ± 2.8	9.28 ± 7.34

3.5 Charge fluctuations

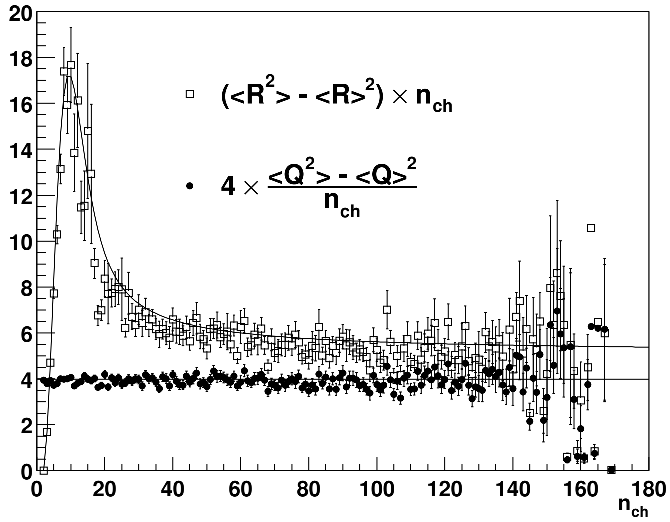

Figure 7. The normalized variances $4v(Q)$ and $v(R)$ as functions of the number of charged particles detected. The curves show the expectations for stochastic behavior. The data are PHENIX preliminary.

There have been suggestions [28–30] that the the fluctuations in the net charge (total positive - negative particles) in a finite detector acceptance can be a signal for the formation of a quark gluon plasma. The basic idea is that when the charge is distributed in the form of quarks, which have less than integer charge, rather than hadrons, the charge is more uniformly distributed in the collision zone. The result could be fluctuations in the net charge which are smaller than expected for a hadron gas.

This measurement is straightforward, but some of the details of the interpretation are not. One question is how and why these fluctuations from the QGP phase survive the transition back to hadronic matter [31,32]. Decay of hadronic resonances can also influence fluctuations. Finally, global charge conservation plays a role for large acceptances. The measurements can be studied in terms of the ratio of positive to negative particles in an event ($R = n_+/n_-$) or in terms of the net charge ($Q = n_+ - n_-$) [28].

In a stochastic scenario, the variance of the net change is

$$V(Q) \equiv \langle Q^2 \rangle - \langle Q \rangle^2 = n_{ch} \tag{7}$$

and the normalized variance is

$$v(Q) \equiv \frac{V(Q)}{n_{ch}} = 1, \tag{8}$$

where n_{ch} is the total number of charged particles detected. The charge ratio, $V(R)$ approaches 4/n_{ch} as n_{ch} increases or $v(R) \equiv n_{ch}V(R)$ asymptotically approaches 4. PHENIX sees a small excess of positive charges – a combined effect of the isospin asymmetry in the initial Au+Au system and background particles produced in secondary interaction in the detector. This excess has a much larger influence on the charge ratio than on the change difference. Figure 7 shows the PHENIX preliminary results for both $v(R)$ and $4v(Q)$. For large n_{ch}, both should approach 4. Also shown in Figure 7 are lines from a calculation assuming stochastic emission (and assuming an excess of positive charges). The curves agree well with the data. $v(Q)$ appears indpendent of multiplicity and is an easier variable to work with. $v(Q)$ is not exactly 1 (it is $\approx$ 0.965), but it is far from the most optimistic of the QGP predictions $v(Q) \approx$ 0.2 [28]. The small deviations from $v(Q) = 1$ are consistent with RQMD simulations and are apparently the result of hadronic decays and global charge conservation. In summary, within the limited acceptance of the PHENIX central arms ($|\eta| < 0.35$), the data show either that the QGP is not present or that the signal does not survive the transition back to hadronic matter.

4. Discussion and Conclusions

A large collection of different measurements have been shown. Each of the measurements was performed with the hope of finding a signal for the quark-gluon plasma. The charge fluctuation measurements seem inconsistent with a model which assumes the presence of a quark-gluon plasma. Furthermore, there are no large non-statistical fluctuations in the mean e_T and mean p_T distributions. The large measured elliptic flow (i.e. v_2 is large) would be expected if a QGP was formed, but it does not prove the presence of the QGP. The large emission times, measured from the difference of R_O and R_S, expected from two-particle correlations if a QGP was formed are not seen. In fact the observation that $R_O \approx R_S$ is inconsistent with most models of relativistic heavy ion collisions – without or without the QGP. The result is a mixed collection of data which neither uniformly support nor oppose the presence of the QGP.

References

[1] Axel Dress, this conference.
[2] Julia Velkovska, this conference.
[3] David Silvermyr, this conference.
[4] K. Adcox *et al.* (PHENIX Collaboration), Phys. Rev. Lett. **86**, 3500 (2001).
[5] K. Adcox *et al.* (PHENIX Collaboration) Phys. Rev. Lett. **87**, 052301 (2001).
[6] K. Adcox *et al.* (PHENIX Collaboration), Phys. Rev. Lett. **88**, 022301 (2001).
[7] E. Kistenev et.al., *Proc. 5th Int. Conf. on Calorimetry in HEP*, World Scientific (1994), pp. 211-223; G. David *et al.*, IEEE Trans. Nucl. Sci. **45**, 692, 705 (1998).
[8] S. Wang *et el.*, Phys. Rev. C**44**, 1091 (1991).
[9] R. Lacey *et el.*, Phys. Rev. Lett. **70**, 1224 (1993).

[10] K. H. Ackermann *et el.* (STAR Collaboration), Phys. Rev. Lett. **86**, 402 (2001).
[11] I. Park *et el.* (PHOBOS Collaboration), Nucl.Phys. A**698**, 564c (2002).
[12] K. Adcox *et al.* (PHENIX Collaboration), nucl-ex/0201008, submitted to Phys. Rev. Lett.
[13] S. Pratt, Phys. Rev. Lett. **53**, 1219 (1984).
[14] G. Bertsch and G.E. Brown, Phys. Rev. C**40**, 1830 (1989).
[15] I.G. Bearden *et al.* (NA44 Collaboration), Phys. Rev. C**58**, 1656 (1998).
[16] R. Soltz, M.D. Baker, J.H. Lee, for E802 Coll., Nucl. Phys. **A661**, 439 (1999); L. Ahle *et al.*, to be submitted to Phys. Rev. C, (2002).
[17] M. Lisa *et al.*, Phys. Rev. Lett. **84**, 2798 (2000).
[18] C. Adler *et al.* (STAR collaboration), Phys. Rev. Lett. **87**, 082301 (2001).
[19] L. Ahle *et al.*, Phys. Rev. C**57**, R466 (1998); D. B. Back *et al.*, Phys. Rev. Lett. **85**, 3100 (2000).
[20] A.N. Makhlin and Y.M. Sinyukov, Z. Phys. **C39**, 69 (1988).
[21] U. Wiedemann, P. Scotto, U. Heinz, Phys. Rev. C**53**, 918 (1996).
[22] S. Mrowczynski, Phys. Lett. **B314**, 118 (1993).
[23] M. Stephanov *et al.*, Phys. Rev. Lett. **81**, 4816 (1998).
[24] A. Dimitru and R. Pisarski, Phys. Lett. **B504**, 282 (2001).
[25] H. Heiselberg, Phys. Repts. **351**, 161 (2001).
[26] H. Appelshauser *et al.*, Phys. Lett. **B459**, 679 (1999).
[27] Z. Ahammed (STAR Collaboration), talk at this conference.
[28] S. Jeon and V. Koch, Phys. Rev. Lett. **85**, 2076 (2000); M. Bleicher, S. Jeon and V. Koch, Phys. Rev. **C62**, 061902(R) (2000).
[29] M. Asakawa, U. Heinz and B Müller, Phys. Rev. Lett. **85**, 2072 (2000).
[30] H. Heiselberg and A. D. Jackson, Phys. Rev. **C63**, 064904 (2001).
[31] E. V. Shuryak and M. A. Stephanov, Phys.Rev. **C63**, 064903 (2001).
[32] K. Fialkowski and R. Wit, Europhys. Lett. **55** (2), 184 (2001).